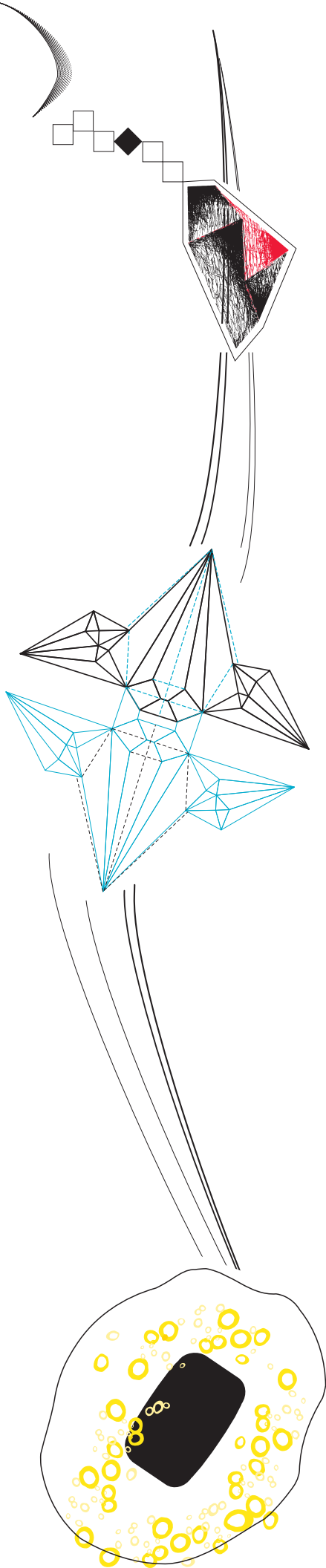




## Internship report

Lisa Deijlen  
UT: s1189697, UMID: 70298724

November 4, 2017



**UNIVERSITY OF TWENTE.**



# Preface

---

This report describes the thirteen weeks I have conducted research at the University of Michigan under the chair of Prof. Steven L. Ceccio. This research internship was performed in partial fulfillment of the degree Mechanical Engineering at the University of Twente.

An internship is the perfect opportunity to explore a work environment in a different country and broaden knowledge about cultures and opinions. I am very grateful for the support of prof. Harry W.M. Hoeijmakers and prof. Steven L. Ceccio in arranging this experience.

During this internship I had the pleasure to work with Juliana Wu, Anubhav Bhatt and in particular with Dr. Harish Ganesh on the subject cavitation. They were always prepared to share their expertise, experimental data and results which led to a very productive use of the limited time I had.

Furthermore, I would like to thank everyone who has contributed to this wonderful experience. In particular the people in rooms AL2010 and AL2016, who immediately included me into their group. The fierce discussions, jokes and small talk made an amazing environment to work in.



# Abstract

---

Young and Holl (1966) studied the effect of cavitation on the wake behind a symmetric wedge. They discovered that the shedding frequency from the far wake, the von Karman vortex street, nondimensionalized as the Strouhal number ( $St$ ) is constant at high cavitation numbers ( $\sigma$ ), but increases, peaks and then decreases again when the cavitation number decreases. The same has been confirmed by Belahadji et al. (1995), who also discovered that the spacing of the vortices, height over distance, changes for cavitation numbers. The physical mechanisms responsible for the observations have yet to be determined.

To understand this behavior several experiments are conducted in a water tunnel. Here, the cavitation number is varied by reducing the pressure in the tunnel and the flow in the wake is visualized using high-speed videos and X-ray densitometry. By my recommendation, experiments were also done with an injection of milk to achieve better visualization of the vortices, especially at higher cavitation numbers.

From these images the vortex spacing, velocity of the vortices and the Strouhal number are obtained. For high cavitation numbers ( $\sigma > 2.5$ ) this has been done using a MATLAB script to detect the vortices, finding the centers and calculating the values. Unfortunately, for smaller cavitation numbers air bubbles caused too much noise to use this automated script and thus the vortices needed to be counted by hand using MATLAB `ginput` command. The results for the vortex spacing ratio (vertical/horizontal spacing) against the cavitation number have a similar behavior as the Strouhal number.

To better understand the properties of a cavitating wake, from both Strouhal number and spacing perspective, the properties of the von Karman vortex street were examined by Saffman and Schatzman (1981) using an inviscid model for the vortex street which modeled the dependence of the vortex spacing with the drag coefficient for a given vorticity ratio between the far wake and shear layer. The insight from their analysis is used to understand the effect of cavitation in altering the vortex spacing and Strouhal number.

Since the drag on the object was not measured, the cavitation numbers from the experimental results are used to calculate the corresponding drag coefficients. The drag coefficients are calculated using the Riabouchinsky model including a correction for the wall effects.

With the help of estimated drag and measured vortex spacing, the experimental results are compared with the theoretical analysis of Saffman and Schatzman (1981). With the assumption of a constant vorticity and velocity in the shear layer for different cavitation numbers it is possible to draw conclusions about the vorticity. Until the Strouhal peak ( $\sigma = 2.05$ ) the vorticity of the vortices decreases and after the peak the vorticity will stay approximately constant. This indicates that the presence of cavitation will influence the wake dynamics behind a wedge. The amount of influence needs to be investigated in further research.



# Contents

---

<b>Preface</b>	<b>i</b>
<b>Abstract</b>	<b>iii</b>
<b>1 Introduction</b>	<b>1</b>
<b>2 Background information</b>	<b>3</b>
2.1 Cavitation . . . . .	3
2.2 Vortex shedding . . . . .	3
2.3 Strouhal number . . . . .	4
2.4 Saffman and Schatzman’s model . . . . .	5
<b>3 Experiments</b>	<b>9</b>
3.1 Experimental setup . . . . .	9
3.2 Data collection . . . . .	10
<b>4 Drag coefficient</b>	<b>13</b>
4.1 Cavity-flow models . . . . .	13
4.1.1 Open wake model . . . . .	13
4.1.2 Riabouchinsky model . . . . .	14
4.1.3 Re-entrant jet model . . . . .	14
4.2 Wall correction . . . . .	15
<b>5 Results</b>	<b>17</b>
5.1 Velocity and spacing . . . . .	17
5.2 Experiments combined with the inviscid model . . . . .	18
<b>6 Conclusion and Discussion</b>	<b>21</b>
6.1 Conclusion . . . . .	21
6.2 Discussion . . . . .	21
<b>A Equations Saffman and Schatzman (1982)</b>	<b>23</b>
<b>B Model comparison with Saffman and Schatzman (1982)</b>	<b>25</b>
<b>C Influence of the energy dissipation factor <math>\epsilon</math> on the inviscid model</b>	<b>29</b>
<b>Bibliography</b>	<b>31</b>



## Introduction

---

Cavitation occurs when a liquid is subjected to a rapid pressure drop. The liquid is abruptly converted into vapor when the pressure drops below the vapor pressure creating cavities in the flow. When these cavities are subjected to higher pressures they will implode and can generate intense shock waves. This creates problems like significant damage to moving parts, noise and decrease of performance and thus an engineering interest is triggered to fully understand this phenomenon.

Placed in a fluid stream, bluff objects will experience a separated flow extending to their wake. The detachment of the boundary layer on both upper and lower surfaces forms two shear layers that depending on the Reynolds number, will shed into alternating vortices also known as the von Kármán vortex street. It is of high importance to predict the properties of vortex shedding in the street accurately. When the vortex shedding frequency lies close to a resonance frequency of a nearby mechanical system large deflections and fatigue cracks are likely to occur leading to premature failure.

The vortex street wake structure behind a bluff object for low Reynolds numbers is well known and has been studied by Roshko (1955), Gerrard (1978) and Strykowski and Sreenivasan (1990). However, the effect of cavitating flows has only been studied by a few. Young and Holl (1966) have discovered that the vortex shedding frequency, and thus Strouhal number, at low cavitation numbers increases until a certain point and then decreases again with a decreasing cavitation number. Similarly, Belahadji et al. (1995) showed that the Strouhal number and the distance between the two rows of primary vortices is influenced by the cavitation. Young and Holl (1966) and Belahadji et al. (1995) discovered and confirmed the existence of a peak in Strouhal number for a decreasing cavitation number. However, the physical mechanisms behind this behavior are yet unknown and is the primary motivation for this research.

Saffman and Schatzman (1982) created an inviscid model for the von Kármán vortex street wake related to the wake behind a bluff body. This model studied the dependence of the vortex spacing with the drag coefficient for a given vorticity ratio. This model is used to connect the effect of a changing cavitation number to the vorticity of the vortices in the fully developed vortices.

First chapter 2 will give some background information for this research topic. Chapter 3 gives an overview of the experimental setup used for the experiments and the methods used to gather data from these experiments. Because Saffman and Schatzman's model uses the drag coefficient, different models were investigated in chapter 4 to determine the drag coefficient for the experiments. The results of the experiments and the comparison with Saffman and Schatzman's model are given in chapter 5. Lastly the results will be discussed in chapter 6 and possibilities for future work are given.



## Background information

---

To truly understand the behavior of the vortex street in cavitating flows it is necessary to first understand what cavitation is and how the vortex street originates. Furthermore, the inviscid model of Saffman and Schatzman (1982) is discussed since this model will be used to compare to the experimental results.

### 2.1 Cavitation

When the local pressure drops below the vapor pressure a liquid will evaporate. This process can be compared to boiling water but instead of a constant pressure and an increasing temperature, the pressure is reduced and the temperature is constant. This process of forming vapor cavities is called cavitation. When these low pressure vapor cavities are subjected to higher pressures elsewhere in the flow, the cavities implode and can generate intense shock waves. This research will focus on hydrodynamic cavitation which describes the cavitation process in a flowing liquid.

The potential of a flow to cavitate can be described by the free stream cavitation number  $\sigma$  and can be calculated with equation 2.1. It gives a relationship between the free stream pressure,  $p_\infty$ , the vapor pressure,  $p_v$ , the density of the liquid,  $\rho$  and the free stream velocity,  $U_\infty$ . When a flow has a low cavitation number it only takes a small pressure fluctuation for cavitation to occur. A flow with a larger cavitation number will need a much bigger pressure drop for this to happen. It is thus much more likely that cavitation is going to occur in a flow with a low cavitation number than in a flow with a high cavitation number.

$$\sigma = \frac{p_\infty - p_v}{\frac{1}{2}\rho U_\infty^2} \quad (2.1)$$

Behind a bluff object a low pressure region is produced by the separated shear flows. Whenever this pressure is low enough, the region will be filled with vapor forming a cavity. This is called partial cavitation, figure 2.1a. The shape and size of this cavity is determined by the geometric parameters of the object and the free stream cavitation number. As the cavitation number is decreased the finite-length cavity grows in length and ultimately grows into a super cavity, figure 2.1c.

### 2.2 Vortex shedding

Re-entrance of the flow into the cavity leads to the shedding of vapor clouds. In an ideal steady flow the stagnation point will lie in the middle of the after wake on the wake axis of figure 2.2. However, in reality, due to the unsteady separation of the flow around a blunt object this stagnation point is highly unstable and will move up and down the wake axis.

The re-entrant jet from stagnation point  $s$ , figure 2.2, locks in a part of the vapor liquid mixture inside the cavity and then sheds this vapor cloud from the cavity. During the actual shedding the stagnation point  $s$  moves with the re-entrant jet to the other side of the wake axis. This alternates

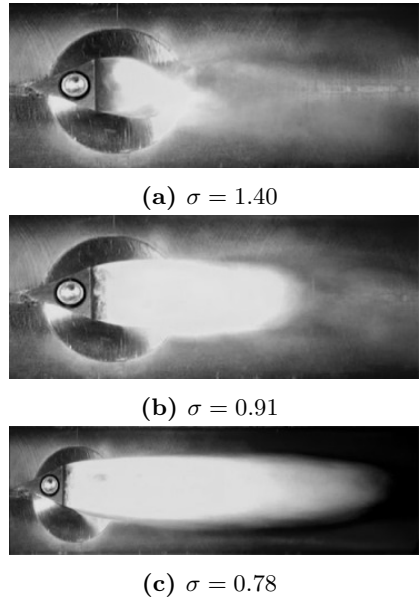


**Figure 2.1:** *Partial and super cavity in the wake of a 45° wedge with  $U_\infty = 9.4$  [m/s]. (Pictures from Ahn et al. (2012))*

between a re-entrant jet from the upper and lower flow creating a train of alternating vortices also known as a von Kármán street.

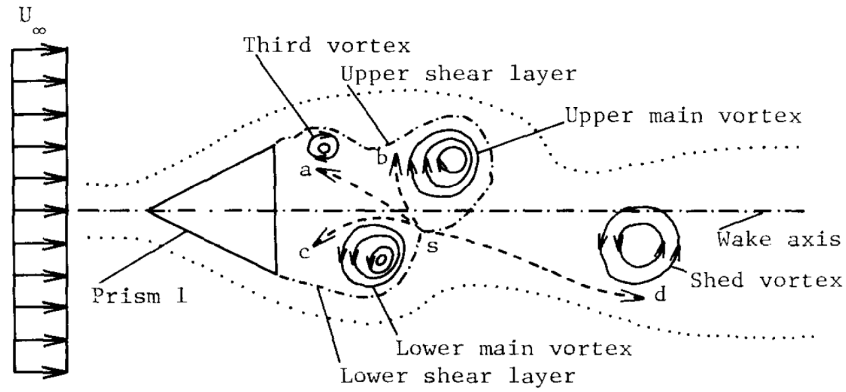


**Figure 2.2:** *Shedding mechanism behind a wedge (from Nakagawa (1989)).*

### 2.3 Strouhal number

An important dimensionless number describing vortex shedding is the Strouhal number,  $St$ . The Strouhal number represents the ratio of the inertial forces to the unsteadiness of the flow and is given in equation 2.2 with the frequency of vortex shedding  $f$ , characteristic length  $L$  (in these experiments the wedge height) and flow velocity  $U_\infty$ .

$$St = \frac{fL}{U_\infty} \quad (2.2)$$

Young and Holl (1966) discovered a relationship between the Strouhal number and the cavitation number, figure 2.3. The Strouhal number is constant for high cavitation numbers. However with a decreasing cavitation number the Strouhal number increases, has a peak and then decreases again. Similar behavior is seen for different angles of a wedge.

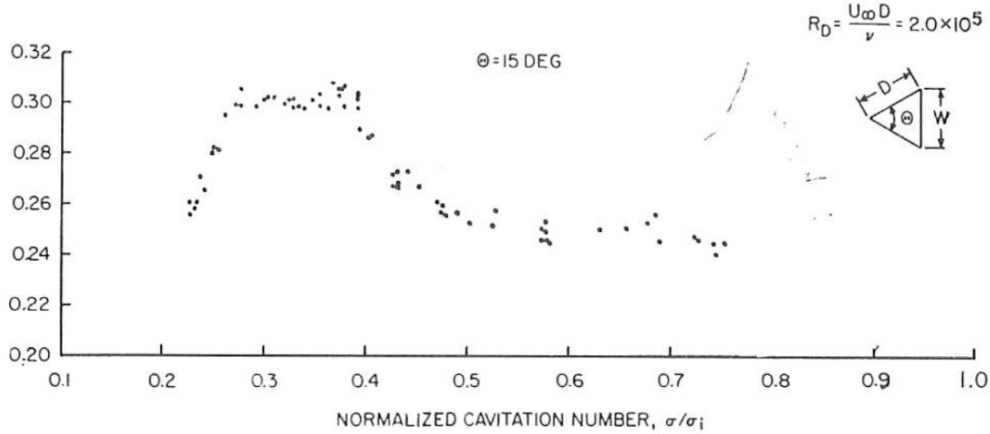


**Figure 2.3:** *Strouhal number versus normalized cavitation number (from Young and Holl (1966)).*

Belahadji et al. (1995) confirmed the existence of this Strouhal peak as can be seen in figure 2.4a. In figure 2.4b they also showed the effect of cavitation on the physical properties of the Kármán vortex street. Here it can be seen that the vertical vortex spacing  $B$  over the horizontal vortex spacing  $A$  decreases with decreasing cavitation number similar to the Strouhal graph after the peak. The goal of this research is to further investigate the physical interpretation of this Strouhal dependent behavior.

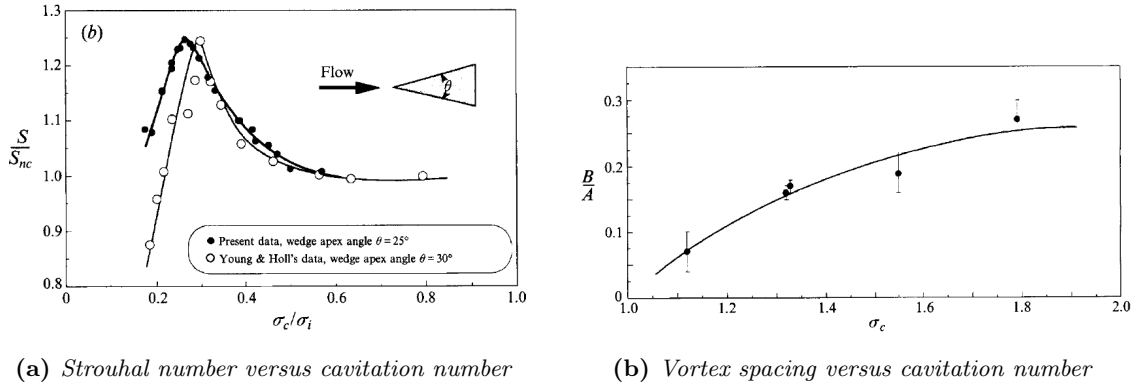


**Figure 2.4:** *Strouhal and vortex spacing of a 25° wedge (from Belahadji et al. (1995))*

## 2.4 Saffman and Schatzman's model

Saffman and Schatzman (1982) created a inviscid model that relates properties of the vortex street with properties of the flow. This is done by deriving three expressions for the momentum, energy and vorticity flux for an inviscid uniform vortex street of finite-area vortices placed in an uniform stream of velocity  $U_0$ . Even though a purely inviscid model is not completely adequate for accurate

predictions for the real case, the goal of the model is to investigate the characteristics of the inviscid flow and see to what extent the properties real flow can be compared.

A graphical representation of an inviscid uniform vortex street of a finite-area vortices  $\Sigma$  is given in figure 2.5. In this figure the following quantities are indicated: the wavelength  $l$ , the spacing of the vortex streets  $h$ , the wedge height  $b$ , the vortex area  $A$ , the vortex strength  $\Gamma$  and direction of the velocities.

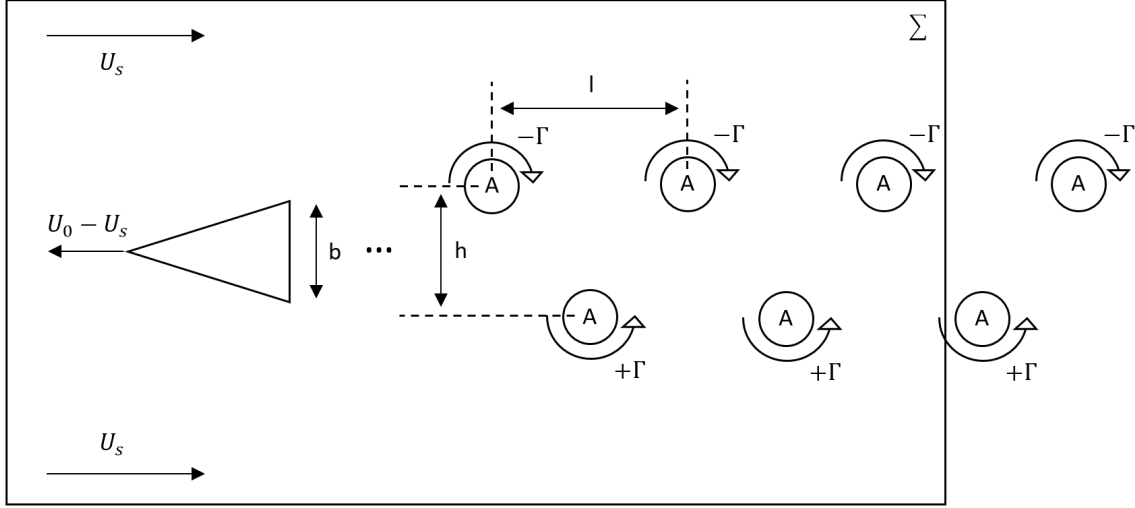


**Figure 2.5:** Sketch of the flow in an fixed region  $\Sigma$  indicating the quantities.

The three non-dimensionalized equations used for the model are:

$$\frac{\kappa \hat{U}_0^2}{2} \left( \frac{C_D}{\beta} \right) = \kappa (\hat{U}_0 - \hat{U}_s) + \hat{D}' \quad (2.3)$$

$$(1 - \epsilon) \frac{\kappa \hat{U}_0^2}{2} \left( \frac{C_D}{\beta} \right) = \hat{T} - \kappa \hat{U}_s \quad (2.4)$$

$$\hat{U}_0 - \hat{U}_s = \frac{1}{2} \delta \hat{U}_0^2 \quad (2.5)$$

The three functions  $\hat{U}_s$ ,  $\hat{D}'$  and  $\hat{T}$  represent respectively the propagation velocity, part of the momentum and the energy of the wake of the uniform vorticity. They are functions of  $\kappa$  and  $\alpha$  and are given in appendix A. The description of these variables together with the parameters of equations 2.3, 2.4 and 2.5 are given in table 2.1.

Equation 2.5 can be used to eliminate  $\hat{U}_0$ ,  $\hat{U}_0 = \frac{1 \pm \sqrt{1 - 2\delta \hat{U}_s}}{\delta}$ , and together with known functions  $\hat{U}_s(\kappa, \alpha)$ ,  $\hat{D}'(\kappa, \alpha)$  and  $\hat{T}(\kappa, \alpha)$  can be plugged into equation 2.3 and 2.4. This results into two equations for  $\kappa$  and  $\alpha$  with parameters  $C_D/\beta$ ,  $\epsilon$  and  $\delta$  which can be solved with MATLAB using a nonlinear least-squares solver (*lsqnonlin*) for given values of the parameters.

After the equations are solved for the two variables  $\kappa$  and  $\alpha$ , two other quantities namely the Strouhal number  $S$ , equation 2.6, and the dimensionless vortex strength  $\hat{\Gamma}$ , equation 2.7, can be determined.

$\kappa$	The ratio of the vortex spacing and wavelength	$(\kappa = h/l)$
$\alpha$	The ratio of the vortex area and the wavelength squared	$(\alpha = A/l^2)$
$\beta$	The ratio of the vortex spacing and the wedge height	$(\beta = h/b)$
$C_D$	The drag coefficient	
$\epsilon$	The fraction of the work done by the body on the fluid that is lost by dissipation in the near wake ('the mechanical efficiency')	
$\delta$	The fraction of vorticity in shear layers that ends up in the fully developed vortices times the square of the ratio of the velocity at the edge of the shear layer to the velocity of the free stream	$(\delta = \omega_v/\omega_s \cdot (U_s/U_\infty)^2)$

**Table 2.1:** Variables and parameters of equations 2.3, 2.4 and 2.5.

$$S\beta = \kappa \frac{\hat{U}_0 - \hat{U}_s}{\hat{U}_0} \quad (2.6)$$

$$\frac{\hat{\Gamma}}{\beta} = \frac{1}{\kappa \hat{U}_0} \quad (2.7)$$

The quantities  $\kappa$ ,  $\alpha$ ,  $S\beta$  and  $\hat{\Gamma}/\beta$  are given for different values of  $\delta$  and  $\epsilon = 0$  (the ideal case) in appendix B with the original figures from Saffman and Schatzman (1982) for comparison. These figures show that the MATLAB program is validated in comparison with the results of Saffman and Schatzman (1982). For this research the figures for  $\kappa$  versus the  $C_D/\beta$  are most used and are given in figure 2.6.

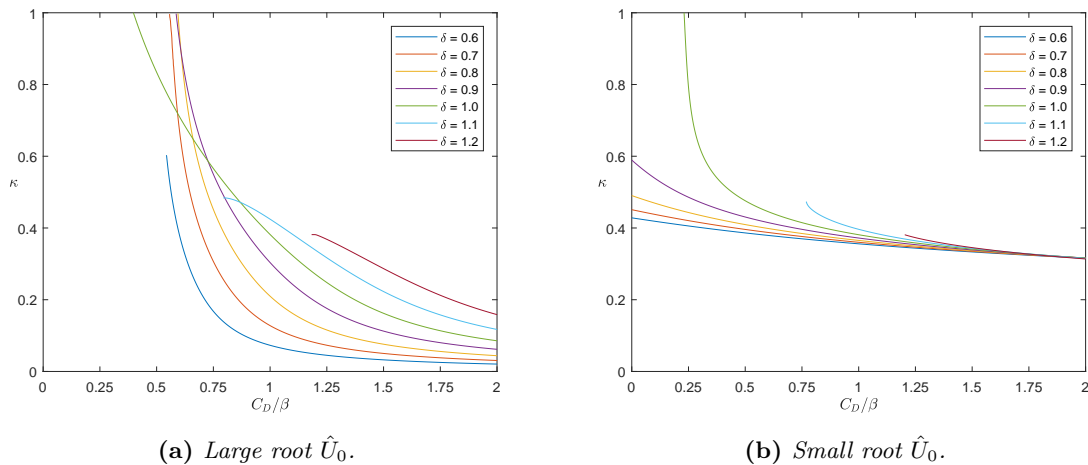


**Figure 2.6:** Spacing ratio of the vortex street as function of the drag coefficient for various values of  $\delta$  and  $\epsilon = 0$ .

The influence of  $\epsilon$  is determined by solving the equations for  $\delta = 0.8, 1.0$  &  $1.2$  and  $\epsilon = 0, 0.3, 0.6$  &  $0.9$ . The quantities  $\kappa$ ,  $\alpha$ ,  $S\beta$  and  $\hat{\Gamma}/\beta$  for these values are given in appendix C. From this can be concluded that  $\epsilon$  mostly influences the vortex area  $\alpha$  and that the other values are almost independent of  $\epsilon$ .

Since the experimental results will only contain the spacing ratio of the vortex street  $\kappa$  and the Strouhal number  $S$ , the influence of  $\epsilon$  can be neglected. Thus the ideal case with  $\epsilon = 0$  will be used to evaluate the experiments.



## Experiments

---

To investigate the physical mechanisms behind the Strouhal peak several experiments were conducted in the water tunnel with different wedges. In a second series of experiments milk was added at the base of the wedge to improve the visualization of the vortices. This provided a significant improvement, particularly at high cavitation numbers.

### 3.1 Experimental setup

The experiments were conducted in the 9 inch water tunnel at the University of Michigan. The tunnel has a 6:1 contraction leading into the test section with a diameter of 22 cm. Then the test section transitions into a square cross section of 21 x 21 cm, which is further reduced to a 7.6 x 7.6 cm cross section test section. The flow velocity in the test section can be varied from 0 to 18 m/s and the static pressure from near vacuum to 100 kPa. For these experiments an approximately constant velocity of 6 m/s has been maintained while varying pressures between 25 and 85 kPa.

Wedges varying an angle of 15 or 30 degrees and a base height of 1.90 or 0.85 cm were used. During this internship experiments were done with the 30 degree small wedge and 15 degree big wedge while injecting milk. Then data were extracted from the high speed images. Experiments without milk were done several months before, however data was extracted from the high speed images during this internship.

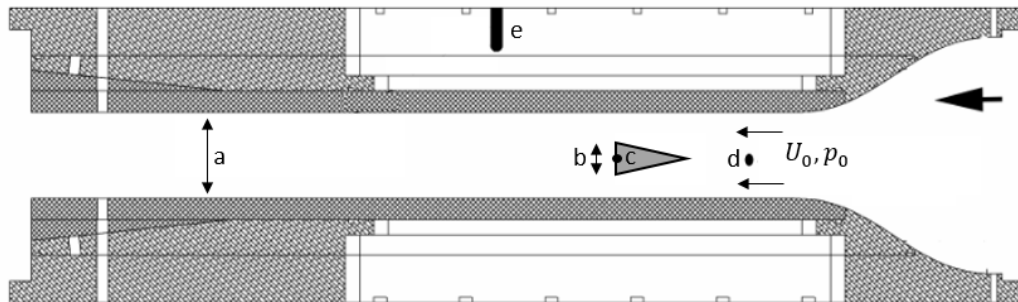


**Figure 3.1:** Schematic overview test section with (a) cross section of 7.6 cm, (b) wedge base height of 1.90 or 0.85 cm, (c) injection port, (d) pressure transducer and (e) hydrophone.

A schematic overview of the test section is given in figure 3.1. At the base of the wedge, point c in figure 3.1, an injection port is placed from which a liquid can be added to the flow. The static pressure is measured with an Omega PX20-030A5V absolute pressure transducer at the entrance of the scaled test section, point d in figure 3.1. The pressure difference between point d and upstream before the reduction was measured with an Omega PX409030DWU10V differential pressure transducer. These measurements together with the area ratios can be used to determine the velocity in point d. On top

of the test section, point e in figure 3.1, a Brüel & Kjær hydrophone type 8103 is placed to record the vortex shedding. The hydrophone is placed in a layer of water on top of the test section, but separated from the test section by a plastic wall.

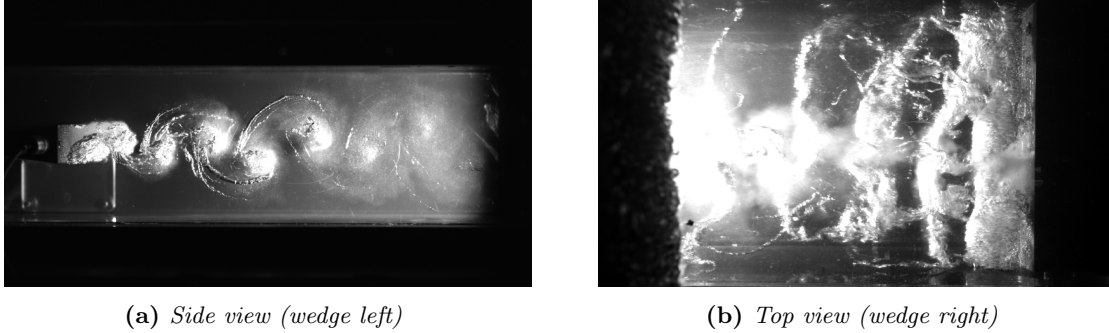


**Figure 3.2:** Side and top view of the test section taken with the Phantom v730 high-speed cameras. (cavitation number  $\sigma = 1.83$ )

The test section is illuminated by two Arrilux lamps and is captured simultaneously from the top and side views by two Phantom v730 high-speed video cameras. The frame rate of the video recordings was 1000 frames per second (fps) for the plain experiments and 500 fps for the milk experiments. The top view camera was fitted with a multiple focal length lens of range 35-55 mm and the side view camera with a 90 mm focal length lens. The cameras were triggered using a TTL signal generated by a Stanford DG-535 delay generator which was triggered manually. They were then synchronized using the Phantom Cine Control software and exported as '.avi' files with 1 fps. A graphical representation of the side and top view is given in figure 3.2.

## 3.2 Data collection

Using the high-speed images the vortex spacing and velocity can be measured. Figure 3.3 shows an example frame for vortex location, the horizontal spacing  $A$  and vertical spacing  $B$ .

Collection of the data has been done with two different MATLAB scripts. Both scripts calibrate the wedge height in pixels with the height in SI units and crop the image to only include the after wake. They differ in collecting the location of the vortices manually or automatically, but besides the difference in input the scripts work in a similar matter.

Manual tracking is very straight forward. The figure opens in MATLAB and the vortex locations are found by clicking on the middle of the vortex with the cursor. The MATLAB function *ginput* saves these values to a vector. This method is very labour intensive and vulnerable to imprecise selection of the vortex centers.

In the automatic tracking script the cropped image is turned into a binary image with a threshold found by trail-and-error. The MATLAB function *regionprops* is then used to find all white areas and centroids. The vortices are detected with a reasonable assumption of the area of the vortices and the corresponding centroids are saved in a vector. This method is very time efficient and thus can generate much more data points than the manual tracking script can. Also the precision of the data is increased since the script will find the exact centroid of the detected vortex.

The automatic tracking script was developed to collect larger and more accurate data sets thus making it ideal to use throughout the whole experiment. However, due to the visual noise of cavitation at low cavitation numbers it is not possible to use this script for cavitation numbers lower than 2.5. This means that for  $\sigma < 2.5$  the manual tracking script has to be used.

After gathering the locations of the vortices in the first frame they are sorted on their horizontal location. In all the following frames the vortex location is matched with the vortex location of the

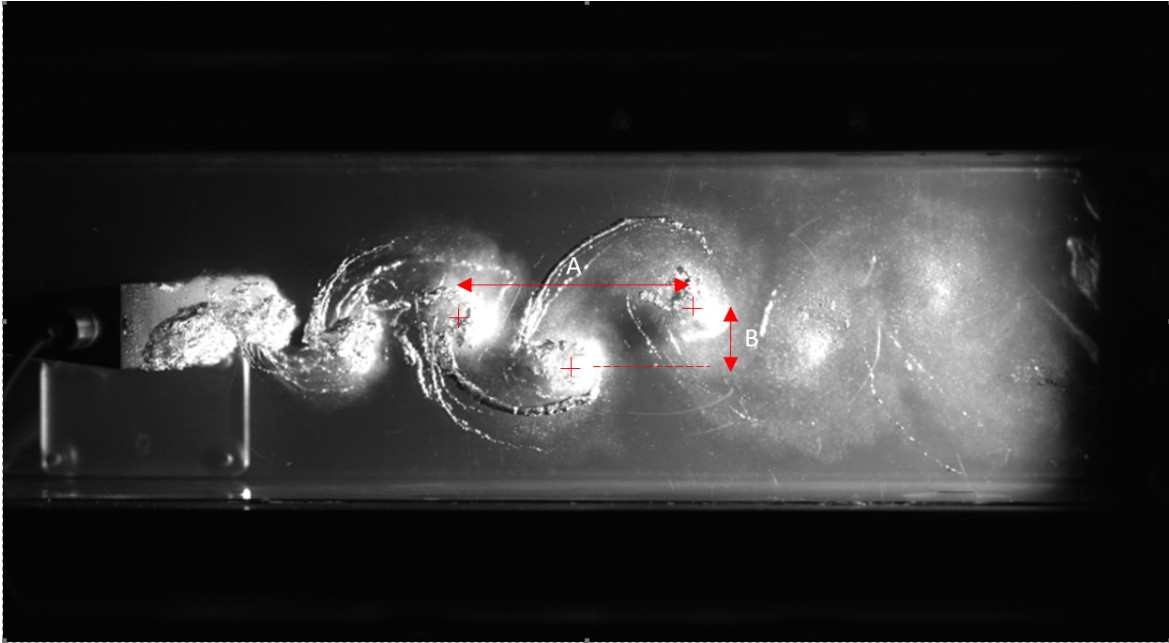


**Figure 3.3:** *Vortex spacing.*

previous frame or added as a newly created vortex to create a matrix of vortices and their path. This matrix is then used to calculate the vortex spacing and velocities.



## Drag coefficient

---

The drag coefficient of the experimental data is needed to interpret the results with the inviscid model of Saffman and Schatzman (1981). Since the drag on the object was not measured, the cavitation numbers from the experimental results are used to calculate the corresponding drag coefficients. Three cavity-flow models were investigated to determine the appropriate drag coefficient. After this, a wall correction was implemented to correct for the assumed unbounded flow of the cavity-flow models.

### 4.1 Cavity-flow models

The cavity-flow models have been examined by Wu et al. (1971). Their work contains the theoretical models as well as experiments done to determine the accuracy of each.

#### 4.1.1 Open wake model

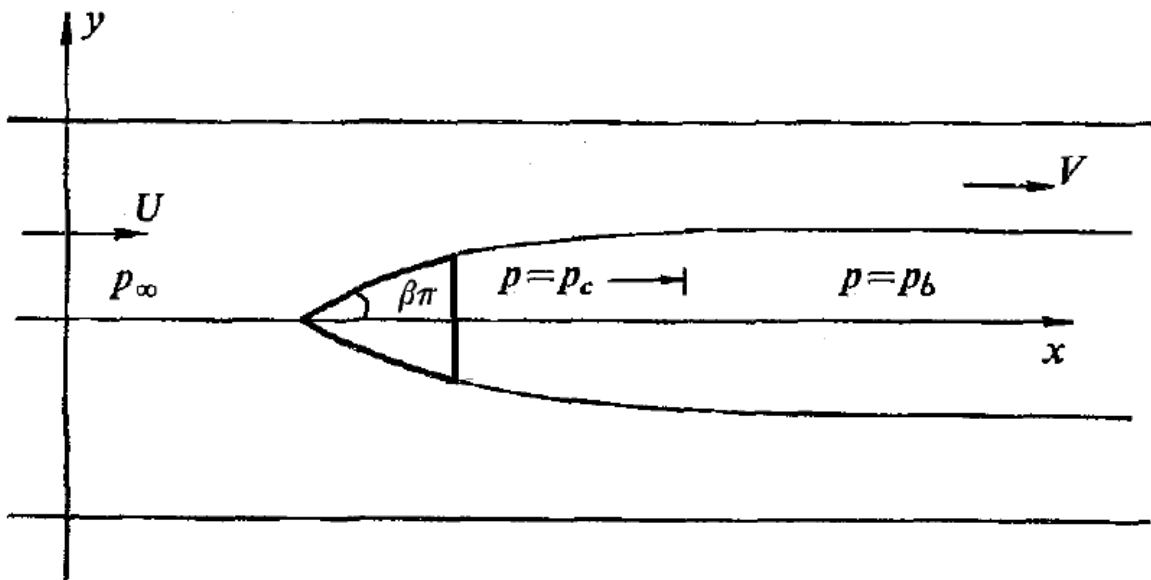


Figure 4.1: Open wake model. Retouched image from Wu et al. (1971).

The open wake model, figure 4.1, assumes that all the flow coming into the tunnel is pushed to the sides and thus  $U < V$ . Since in reality the cavity behind the object is not infinite, the predicted drag coefficient will likely overestimate the true drag coefficient.

### 4.1.2 Riabouchinsky model

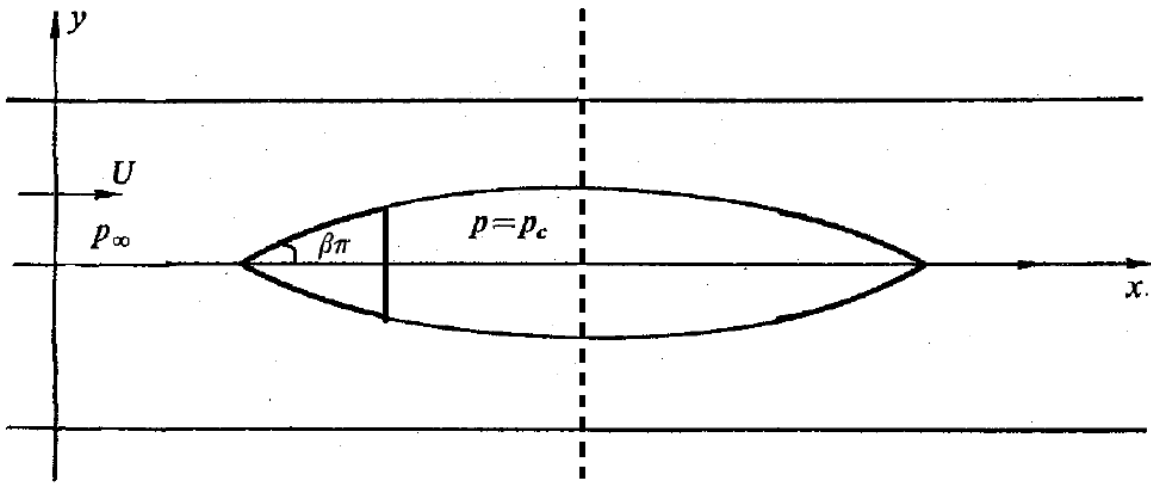


Figure 4.2: Riabouchinsky model. Retouched image from Wu et al. (1971).

The Riabouchinsky model, figure 4.2, considers a finite cavity mirrored to the blunt object over the dotted line. This model has an advantage of providing a point of maximum velocity and minimum pressure to determine the drag coefficient. From experiments done by Wu et al. (1971) it is concluded that the Riabouchinsky model provides a better estimation of drag than the open wake model.

### 4.1.3 Re-entrant jet model

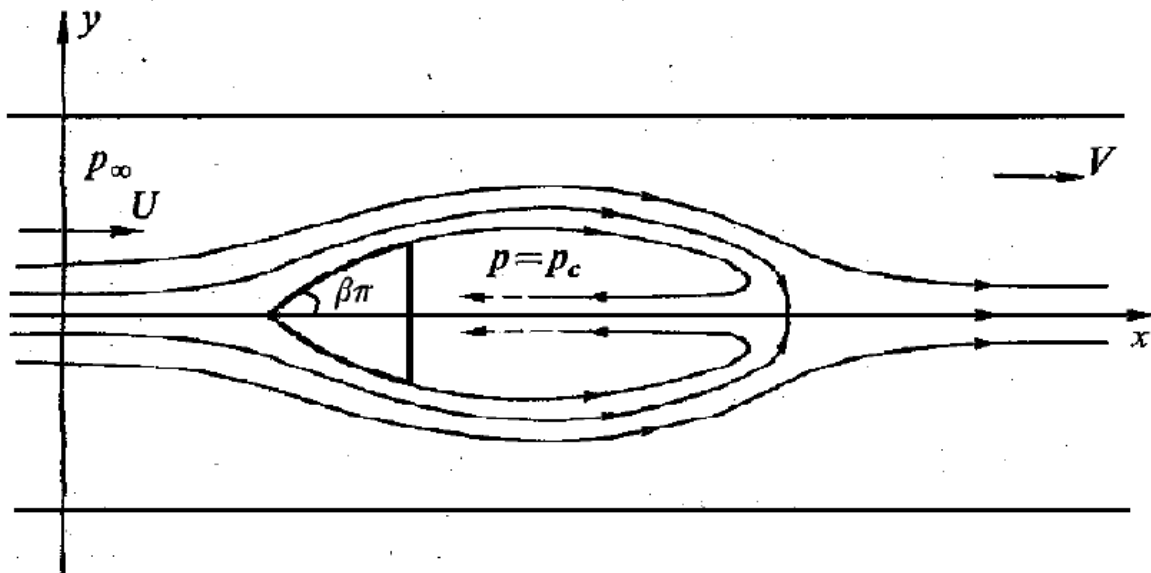


Figure 4.3: Re-entrant jet model. Retouched image from Wu et al. (1971).

The Re-entrant jet model, figure 4.3, assumes that part of the flow will flow back to the bluff object adding a swirling effect to the flow. Of all the mentioned models, this seems the most accurate at first glance, but it is also the most difficult to solve.

Gilbarg (1960) states that even though the Riabouchinsky model and the re-entrant jet model are of great conceptual difference the models give almost identical results in the drag coefficient of wedges. Therefore the Riabouchinsky model has been chosen to determine drag coefficients for the experiments.

## 4.2 Wall correction

The Riabouchinsky model uses the assumption of an unbounded flow. In reality the flow is bounded to the edges of the water tunnel which effects the maximum velocity on the wall and the minimum pressure. The model should be corrected for the wall effects.

The results of the Riabouchinsky model and the correction as described in Wu et al. (1971) are shown in figure 4.4. These results are used in chapter 5 to interpret the results from the experiments.

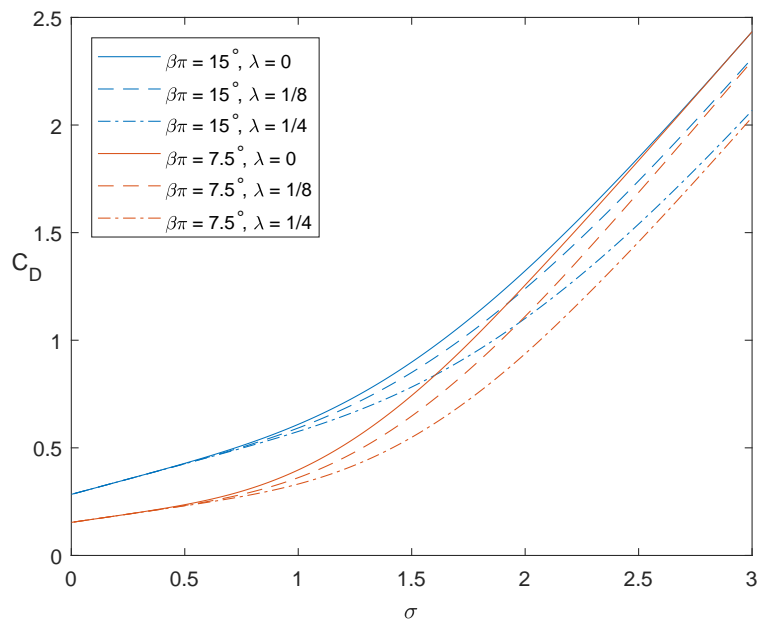


**Figure 4.4:** Riabouchinsky model for the different wedge angles with wall correction for the different wedge heights.

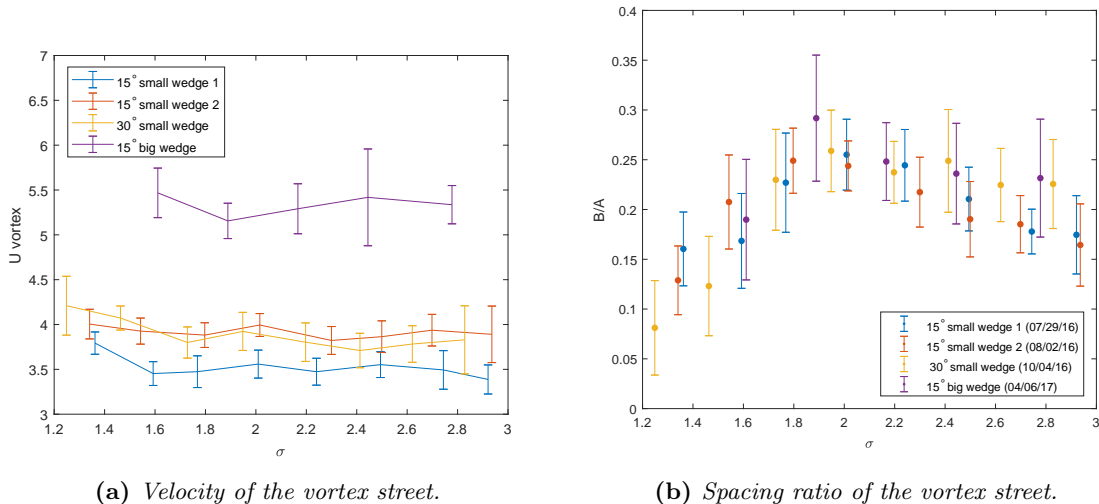


## Results

The behavior of the Strouhal number has been tested and confirmed in earlier experiments done at the University of Michigan. The wake dynamics, in particular the vortex street velocity and spacing, were investigated and compared to the inviscid model of Saffman and Schatzman (1981). During these experiments, two of the three parameters of the Strouhal number,  $U_\infty$  and  $L$ , were kept constant. The vortex shedding frequency is therefore the only parameter that varies throughout the cavitation numbers. Increasing vortex shedding frequencies are in direct connection with an increasing vortex street velocity or/and spacing.

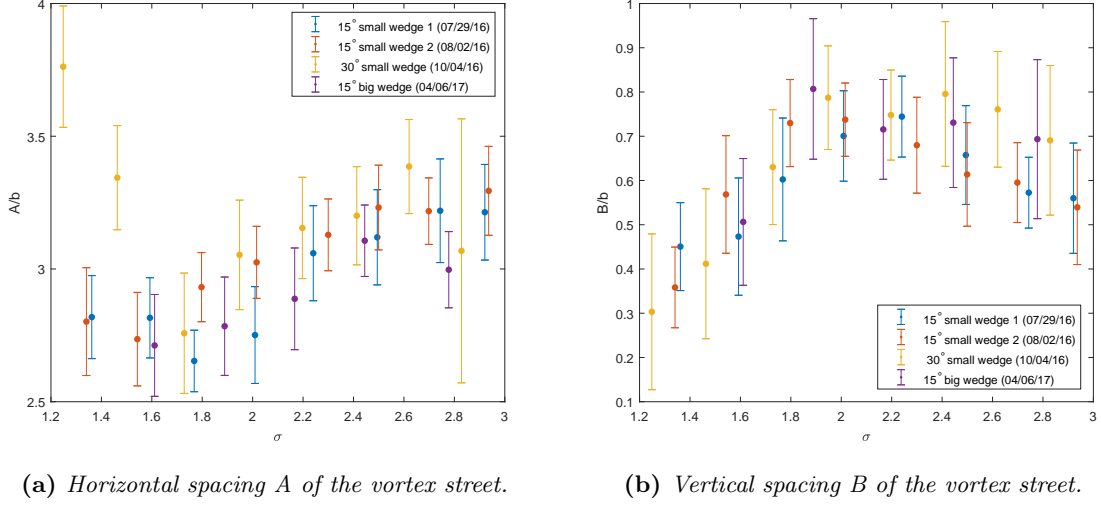
### 5.1 Velocity and spacing

Figure 5.1a shows an approximately constant velocity throughout the cavitation numbers. This would suggest that the distance between the vortices should be affected. The spacing ratio of the vortex street behind a wedge is given in figure 5.1b. From this can be seen that the behavior of the spacing ratio is similar to the behavior of the Strouhal number. The cavitation numbers of the peak values correspond with each other ( $\sigma \approx 2$ ).



**Figure 5.1:** Vortex velocity and spacing ratio as function of the cavitation number.

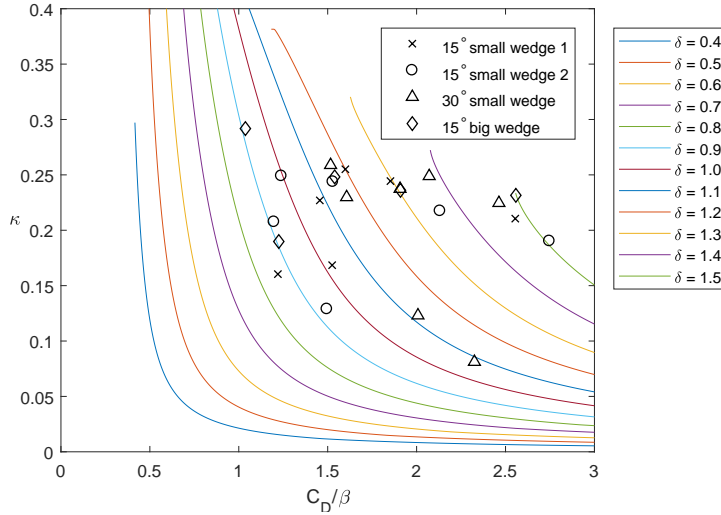
Results for the horizontal and vertical spacing of the vortex street are given in figure 5.2a and 5.2b. It can be seen that both figures have a completely opposite behavior, but in line with the behavior of the Strouhal number. However one might expect a higher increase in horizontal spacing due to the significant frequency drop, figure 5.2a, when decreasing  $\sigma$  after the Strouhal peak ( $\sigma \approx 2$ ).



**Figure 5.2:** Horizontal ( $A$ ) and vertical spacing ( $B$ ) of the vortex street as function of the cavitation number.

## 5.2 Experiments combined with the inviscid model

Experimental data combined with the corresponding drag coefficients can be used with the inviscid model of Saffman and Schatzman (1981). From figure 5.3 can be seen that the data points are scattered over different lines of  $\delta$ . This alone does not provide a lot of information. However adding a legend of the different cavitation numbers, figure 5.4, gives much more insights in the behavior of the after wake.



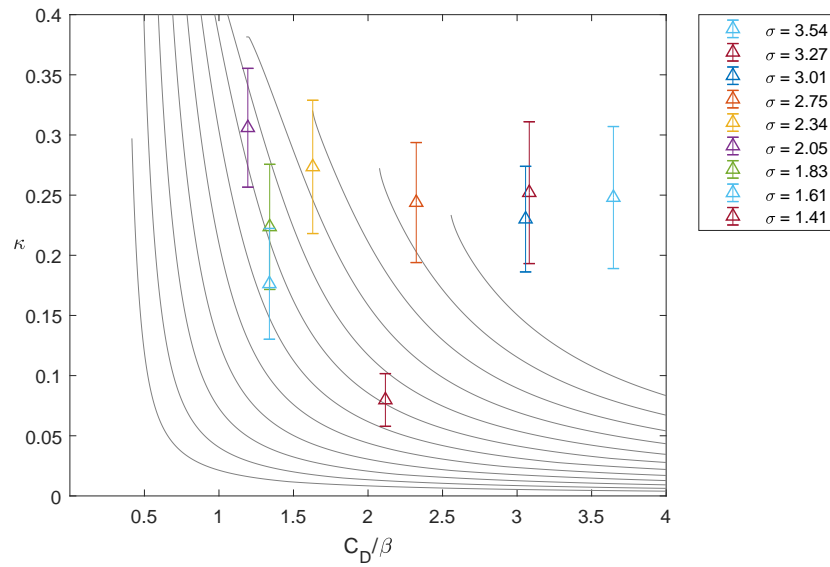
**Figure 5.3:** Experimental data combined with the inviscid model of Saffman and Schatzman (1981).

Figure 5.4 shows that with a decreasing cavitation number,  $\delta$  decreases until the Strouhal peak ( $\sigma = 2.05$ ), after which  $\delta$  stays approximately the same number. The other wedges show a similar behavior.

During the experiments the velocity of the free stream stayed constant and when assuming that the

velocity and vorticity in the shear layer isn't effected by lowering the pressure these are also constant. This means that  $\delta$  would directly be coupled to the vorticity in the fully developed vortices.

With this in mind, figure 5.4 shows that with a decreasing cavitation number the vorticity in the vortices decreases until the Strouhal peak. After the peak the vorticity will stay constant.



**Figure 5.4:** *Experimental data of the 15 degree big wedge on the inviscid model of Saffman and Schatzman (1981) with indication of cavitation number.*



## Conclusion and Discussion

---

### 6.1 Conclusion

From the results it can be seen that the vortex spacing is directly connected to the Strouhal number. Combining this with the theoretical drag coefficient and the inviscid model it can be concluded that the vorticity of the vortex is influenced by the cavitation number. First, for a decreasing cavitation number, the vorticity decreases until the Strouhal peak and then stays constant for smaller cavitation numbers. This indicates that the presence of cavitation in the flow influences the wake dynamics behind the wedge.

### 6.2 Discussion

The physical behavior of the Strouhal number is not yet unraveled, however this research has discovered some interesting aspects that motivate further investigation for a full understanding.

Significant work went into extracting vortex street data from the high speed images. A script was written to save time and collect more data points, however this script was not able to gather all data points from the experiments with a low cavitation numbers. The noise of air bubbles between vortices created too much overlap between vortices so that they could not be seen as separate objects. Due to the time frame of this internship a manual solution was necessary. For future research more time should be put into creating a more robust script to gather a larger volume of more accurate data.

In future research it is recommended to measure the pressure drag over the wedge instead of using theoretical models. When this is done the comparison with the inviscid model would fully be from an experimental point of view, where now it is a combination of experiment and theory.

Currently, effort is directed toward understanding the different mechanisms by which cavitation can cause the observed wake dynamics by redistributing vorticity. One hypothesis is that the shock wave created by the cavitation is causing the behavior of the vortices to change. To test this hypothesis experiments can be done by adding extra gas in the after wake of the wedge suppressing the formation of shock waves. The results of that research can then be compared with the results of this research and conclusions can be made about the influence of cavitation and shock waves on the vortex street properties.



Appendix A

## Equations Saffman and Schatzman (1982)

---

The three expressions for the momentum, energy and vorticity flux in an inviscid uniform vortex street of finite-area vortices placed in an uniform stream of velocity  $U_0$  are given as:

$$\frac{\kappa \hat{U}_0^2}{2} \left( \frac{C_D}{\beta} \right) = \kappa (\hat{U}_0 - \hat{U}_s) + \hat{D}' \quad (\text{A.1})$$

$$(1 - \epsilon) \frac{\kappa \hat{U}_0^2}{2} \left( \frac{C_D}{\beta} \right) = \hat{T} - \kappa \hat{U}_s \quad (\text{A.2})$$

$$\hat{U}_0 - \hat{U}_s = \frac{1}{2} \delta \hat{U}_0^2 \quad (\text{A.3})$$

With non-dimensionalized parameters:

$$\begin{aligned} \kappa &= \frac{h}{l}, \quad \hat{U}_0 = \frac{l}{\Gamma} U_0, \quad C_D = \frac{D}{\frac{1}{2} U_0^2 b}, \quad \beta = \frac{h}{b} \\ \hat{U}_s &= \frac{l}{\Gamma} U_s, \quad \hat{D}' = \frac{l}{\Gamma^2} D', \quad \hat{T} = \frac{l}{\Gamma^2} T \end{aligned}$$

Equation (A.3) can be rewritten so that  $\hat{U}_0$  can be expressed as  $\delta$  and  $\hat{U}_s$ :

$$\hat{U}_0 = \frac{1 \pm \sqrt{1 - 2\delta \hat{U}_s}}{\delta} \quad (\text{A.4})$$

From this can be seen that the model can be solved for two different values of  $\hat{U}_0$  namely the large root  $\left( \hat{U}_0 = \frac{1 + \sqrt{1 - 2\delta \hat{U}_s}}{\delta} \right)$  and the small root  $\left( \hat{U}_0 = \frac{1 - \sqrt{1 - 2\delta \hat{U}_s}}{\delta} \right)$ .

The three functions  $\hat{U}_s$ ,  $\hat{D}'$  and  $\hat{T}$  in equation (A.1) and equation (A.2) were calculated numerically by Saffman and Schatzman (1981) and Schatzman (1981) and were given as a curve fit in Saffman and Schatzman (1982):

$$\hat{U}_s(\kappa, \alpha) = \frac{1}{2} \tanh(\pi\kappa) + a_1 \alpha^2 + a_2 (\alpha^4 + \alpha^6) \quad (\text{A.5})$$

$$\hat{D}'(\kappa, \alpha) = \frac{1}{2\pi} - \kappa \hat{U}_s(\kappa, \alpha) + b_1 \alpha^2 + b_2 \alpha^4 + b_3 \alpha^6 \quad (\text{A.6})$$

$$\hat{T}(\kappa, \alpha) = \frac{1}{2\pi} \left[ \ln \left( \frac{\cosh(\pi\kappa)}{(\pi\alpha)^{\frac{1}{2}}} \right) + \frac{1}{4} \right] + c_1 \alpha^2 + c_2 \alpha^4 \quad (\text{A.7})$$

With parameters:

$$a_1 = \pi^2 \left( \tanh^2(\pi\kappa) - \frac{2}{3} \right) \sinh(\pi\kappa) \operatorname{sech}^3(\pi\kappa)$$

$$a_2 = -120 \left( \tanh^2(\pi\kappa) - 0.412 \right) \left( 1 - 0.82 \frac{\cosh^8(\pi\kappa)}{19.54 + \cosh^8(\pi\kappa)} \right) \operatorname{sech}^2(\pi\kappa)$$

$$b_1 = -\frac{10}{3} \left( \tanh^2(\pi\kappa) - \frac{2}{3} \right)^2$$

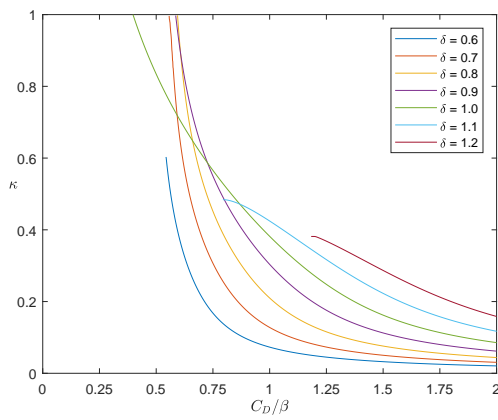
$$b_2 = -\frac{65}{2} \left( \tanh^2(\pi\kappa) - 0.26 \right) \left( 1 - 0.847 \frac{\sinh^8(\pi\kappa)}{\frac{2}{3} + \sinh^8(\pi\kappa)} \right)$$

$$b_3 = 25 \left( 1 - 0.7 \frac{\sinh^8(\pi\kappa)}{\frac{2}{3} + \sinh^8(\pi\kappa)} \right)$$

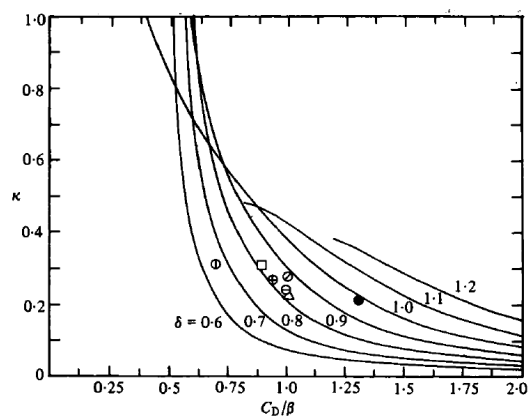
$$c_1 = \frac{5}{6} \left( \tanh^2(\pi\kappa) - \frac{2}{3} \right)^2$$

$$c_2 = \frac{3}{5} \operatorname{sech}(\pi\kappa)$$

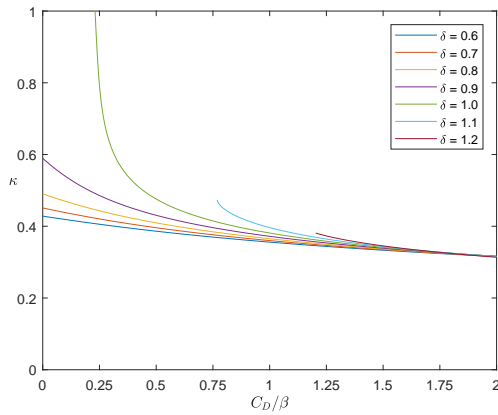
## Model comparison with Saffman and Schatzman (1982)



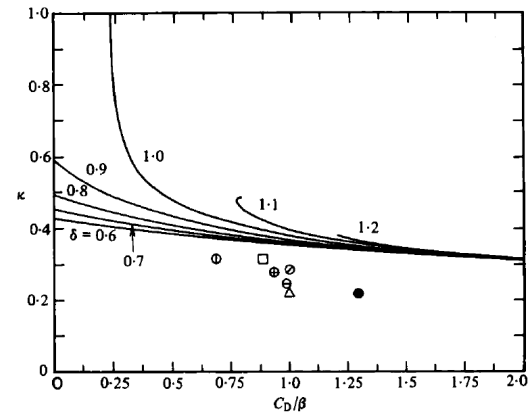
(a) Large root  $\hat{U}_0$ .



(b) Large root  $\hat{U}_0$  by Saffman and Schatzman (1982).

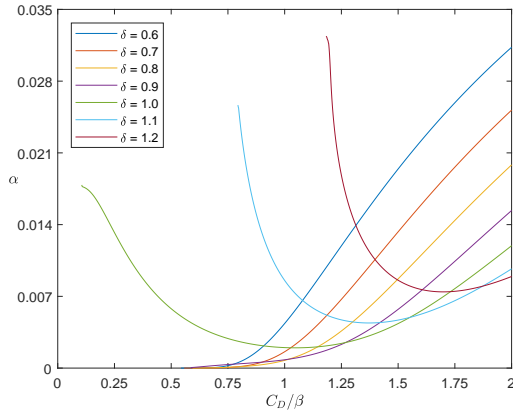


(c) Small root  $\hat{U}_0$ .

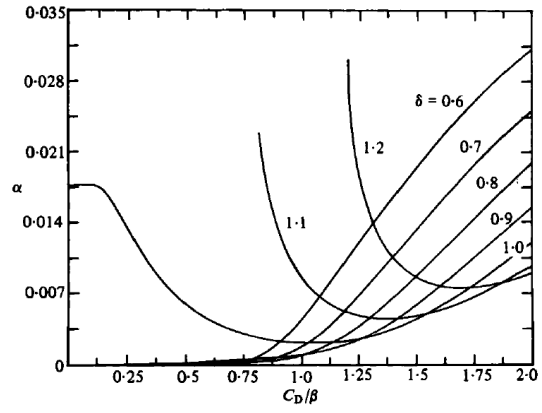


(d) Small root  $\hat{U}_0$  by Saffman and Schatzman (1982).

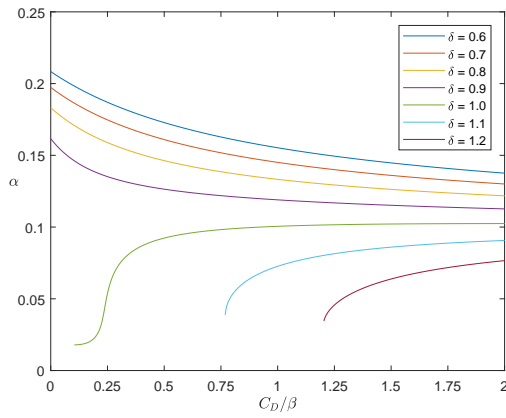
**Figure B.1:** Spacing ratio  $\kappa (=B/A)$  of the vortex street as function of the drag coefficient for various values of  $\delta$  and  $\epsilon = 0$ .



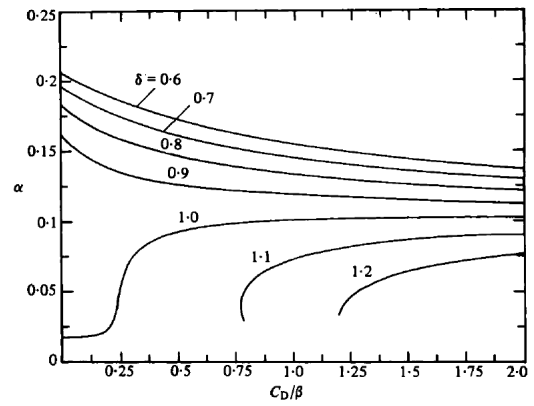
(a) Large root  $\hat{U}_0$ .



(b) Large root  $\hat{U}_0$  by Saffman and Schatzman (1982).

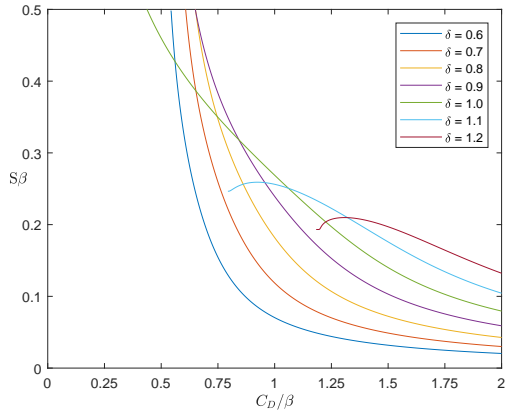


(c) Small root  $\hat{U}_0$ .

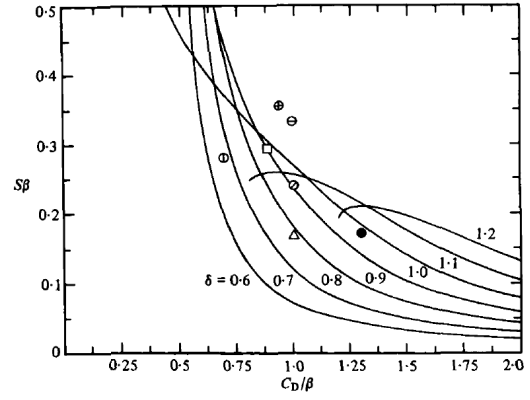


(d) Small root  $\hat{U}_0$  by Saffman and Schatzman (1982).

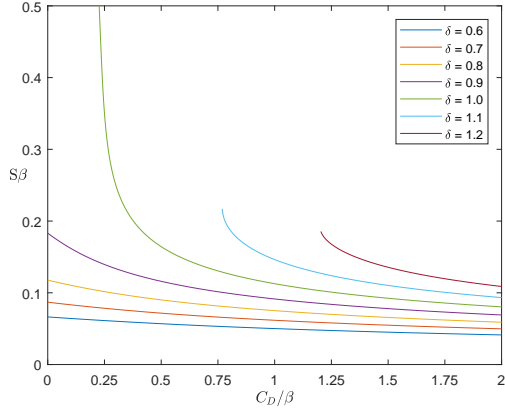
**Figure B.2:** Vortex area  $\alpha$  as function of the drag coefficient for various values of  $\delta$  and  $\epsilon = 0$ .



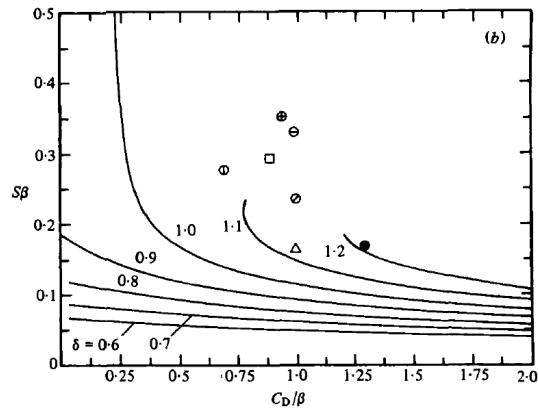
(a) Large root  $\hat{U}_0$ .



(b) Large root  $\hat{U}_0$  by Saffman and Schatzman (1982).

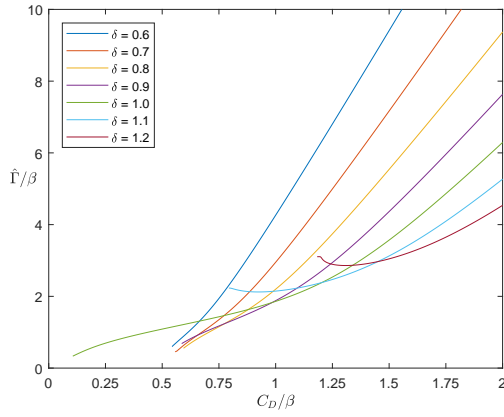


(c) Small root  $\hat{U}_0$ .

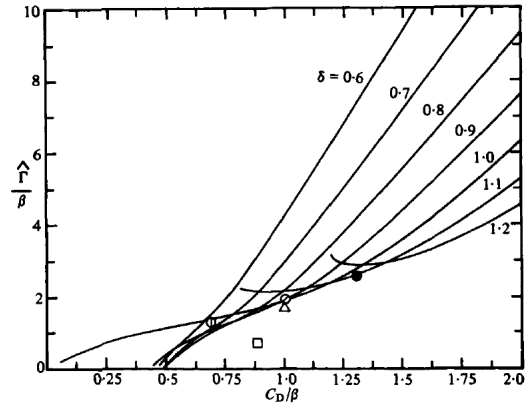


(d) Small root  $\hat{U}_0$  by Saffman and Schatzman (1982).

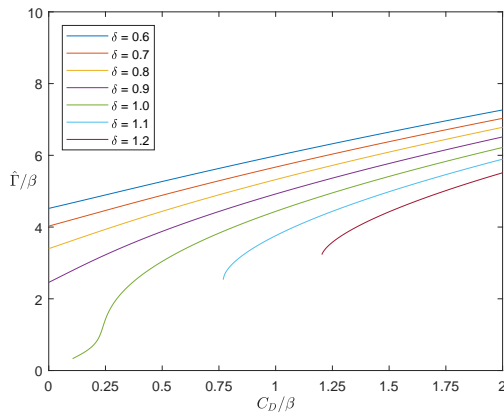
**Figure B.3:** Strouhal number as function of the drag coefficient for various values of  $\delta$  and  $\epsilon = 0$ .



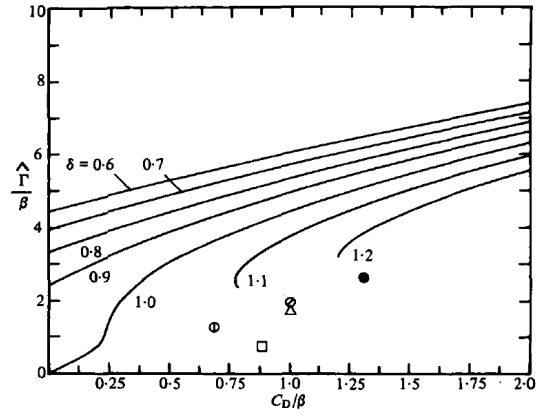
(a) Large root  $\hat{U}_0$ .



(b) Large root  $\hat{U}_0$  by Saffman and Schatzman (1982).



(c) Small root  $\hat{U}_0$ .



(d) Small root  $\hat{U}_0$  by Saffman and Schatzman (1982).

**Figure B.4:** Vortex strength as function of the drag coefficient for various values of  $\delta$  and  $\epsilon = 0$ .

## Influence of the energy dissipation factor $\epsilon$ on the inviscid model

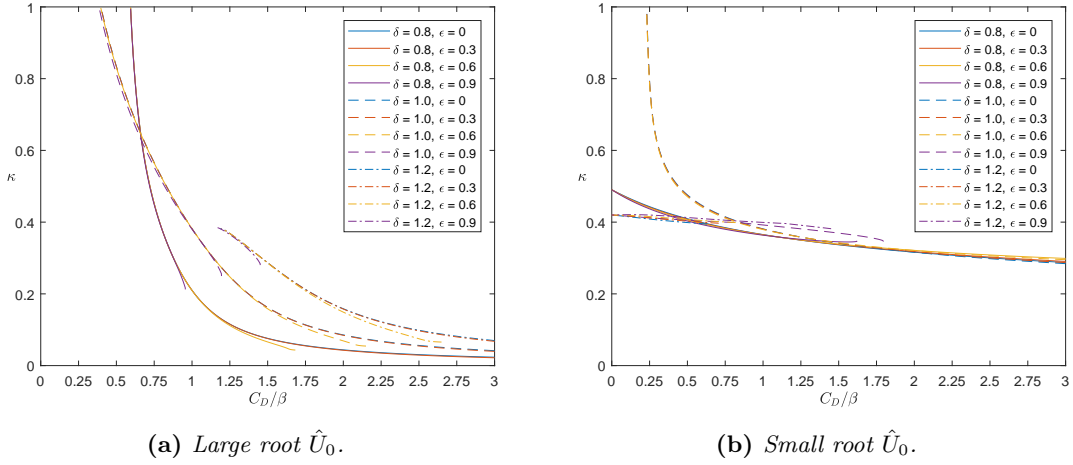


**Figure C.1:** Spacing ratio  $\kappa(=B/A)$  of the vortex street as function of the drag coefficient for  $\delta = 0.8, 1.0$  &  $1.2$  and  $\epsilon = 0, 0.3, 0.6$  &  $0.9$ .

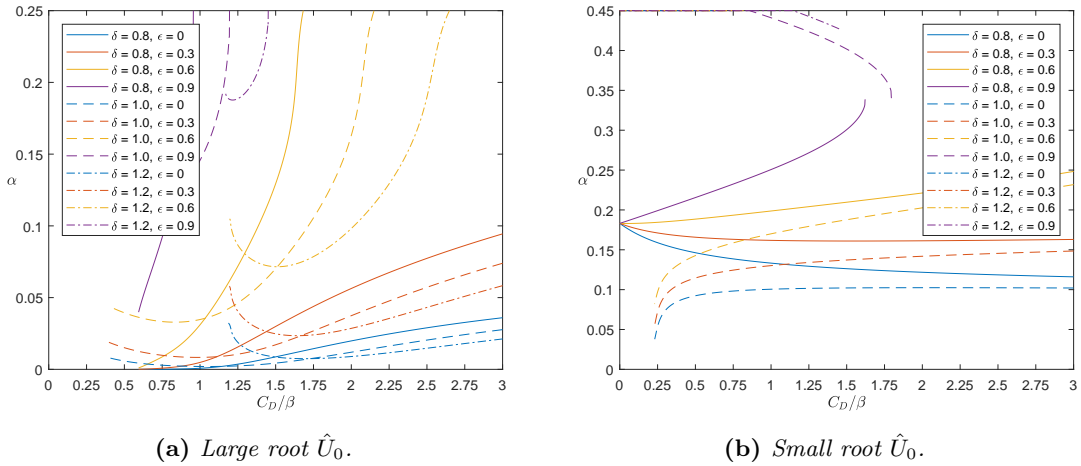
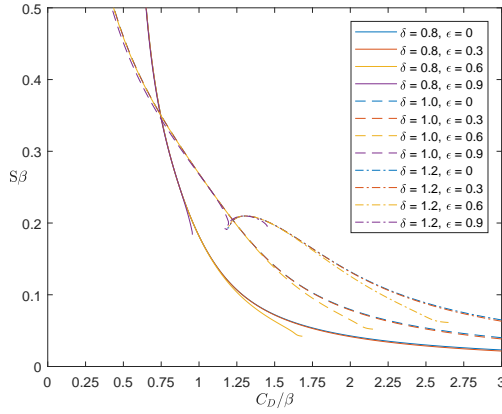
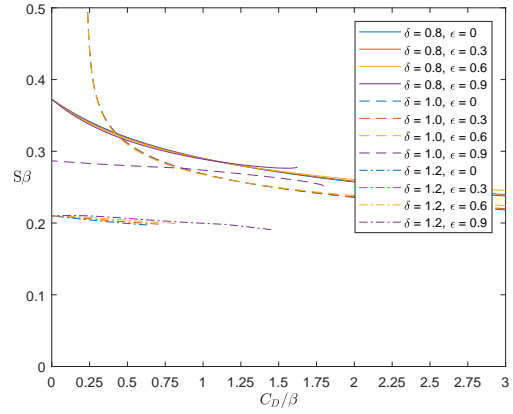


**Figure C.2:** Vortex area as function of the drag coefficient for  $\delta = 0.8, 1.0$  &  $1.2$  and  $\epsilon = 0, 0.3, 0.6$  &  $0.9$ .

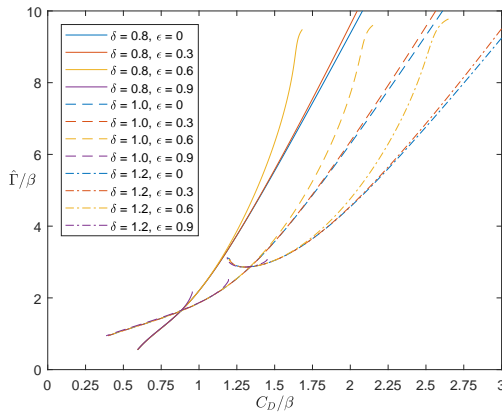


(a) Large root  $\hat{U}_0$ .

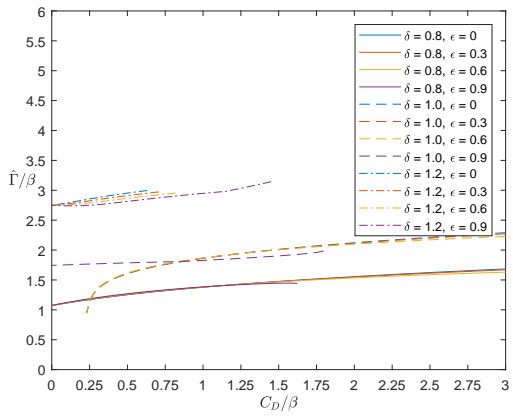


(b) Small root  $\hat{U}_0$ .

**Figure C.3:** Strouhal number as function of the drag coefficient for  $\delta = 0.8, 1.0$  &  $1.2$  and  $\epsilon = 0, 0.3, 0.6$  &  $0.9$ .



(a) Large root  $\hat{U}_0$ .



(b) Small root  $\hat{U}_0$ .

**Figure C.4:** Vortex strength as function of the drag coefficient for  $\delta = 0.8, 1.0$  &  $1.2$  and  $\epsilon = 0, 0.3, 0.6$  &  $0.9$ .

## Bibliography

---

- Byoung-Kwon Ahn, Tae-Kwon Lee, Hyoung-Tae Kim, and Chang-Sup Lee. Experimental investigation of supercavitating flows. *International Journal of Naval Architecture and Ocean Engineering*, 4(2): 123 – 131, 2012.
- B. Belahadji, J.P. Franc, and J.M. Michel. Cavitation in the rotational structures of a turbulent wake. *Journal of Fluid Mechanics*, 287:383–403, 1995.
- J.H. Gerrard. The wakes of cylindrical bluff bodies at low reynolds number. *Philosophical Transactions of the Royal Society of London A: Mathematical, Physical and Engineering Sciences*, 288(1354):351–382, 1978.
- David Gilbarg. Jets and cavities. In *Fluid Dynamics/Strömungsmechanik*, pages 311–445. Springer, 1960.
- Takeo Nakagawa. Vortex shedding mechanism from a triangular prism in a subsonic flow. *Fluid dynamics research*, 5(2):69–81, 1989.
- A. Roshko. On the drag and the wake of bluff bodies. *J Aeronautical Sciences*, pages 124–132, 1955.
- P.G. Saffman and J.C. Schatzman. Properties of a vortex street of finite vortices. *SIAM Journal on Scientific and Statistical Computing*, 2(3):285–295, 1981.
- P.G. Saffman and J.C. Schatzman. An inviscid model for the vortex-street wake. *Journal of Fluid Mechanics*, 122:467–486, 1982.
- J. C. Schatzman. *A model for the Von Karman vortex street*. PhD thesis, California Institute of Technology, 1981.
- P.J. Strykowski and K.R. Sreenivasan. On the formation and suppression of vortex shedding at low reynolds numbers. *Journal of Fluid Mechanics*, 218:71–107, 1990.
- T Yao-Tsu Wu, Arthur K Whitney, and Christopher Brennen. Cavity-flow wall effects and correction rules. *Journal of Fluid Mechanics*, 49(2):223–256, 1971.
- J.O. Young and J. William Holl. Effects of cavitation on periodic wakes behind symmetric wedges. *Journal of Basic Engineering*, 88:163–176, 1966.